

Article

# Fabrication of 3D Gelatin Hydrogel Nanocomposite Impregnated Co-Doped SnO<sub>2</sub> Nanomaterial for the Catalytic Reduction of Environmental Pollutants

Hadi M. Marwani <sup>1,2,\*</sup>, Shahid Ahmad <sup>1</sup> and Mohammed M. Rahman <sup>1,2,\*</sup> 

<sup>1</sup> Chemistry Department, Faculty of Science, King Abdulaziz University, P.O. Box 80203, Jeddah 21589, Saudi Arabia; drchemsci@gmail.com

<sup>2</sup> Center of Excellence for Advanced Materials Research (CEAMR), King Abdulaziz University, P.O. Box 80203, Jeddah 21589, Saudi Arabia

\* Correspondence: hmarwani@kau.edu.sa (H.M.M.); mmrahman@kau.edu.sa (M.M.R.); Tel.: +966-12-6952293 (H.M.M.); Fax: +966-12-6952292 (H.M.M.)

**Abstract:** In the catalytic reduction of various environment pollutants, cobalt-doped tin oxide, i.e., Co-SnO<sub>2</sub> intercalated gelatin (GL) hydrogel nanocomposite was prepared via direct mixing of Co-SnO<sub>2</sub> doped with GL. Then, it was crosslinked internally using formaldehyde within a viscous solution of gelatin polymer, which led to the formation of GL/Co-SnO<sub>2</sub> hydrogel nanocomposite. GL/Co-SnO<sub>2</sub> hydrogel nanocomposite was fully characterized by using field-emission scanning electron microscopy (FESEM), energy dispersive X-ray spectroscopy (EDX), powder X-ray diffraction (XRD), and attenuated total reflection–Fourier transform infrared spectroscopy (ATR-FTIR). The FESEM images indicate that the Co-SnO<sub>2</sub> composite has a spherical structure on the GL matrix while EDX elucidates the elemental composition of each atom in the crosslinked GL/Co-SnO<sub>2</sub> hydrogel nanocomposite. The GL/Co-SnO<sub>2</sub> nanocomposite was checked for the reduction of various pollutants, including 2-nitro-phenol (2-NP), 2,6-dinitro-phenol (2,6-DNP), 4-nitro-phenol (4-NP), Congo red (CR), and methyl orange (MO) dyes with a strong sodium borohydride (NaBH<sub>4</sub>) reducing agent. The GL/Co-SnO<sub>2</sub> nanocomposite synergistically reduced the MO in the presence of the reducing agent with greater reduction rate of 1.036 min<sup>-1</sup> compared to other dyes. The reduction condition was optimized by changing various parameters, such as the catalyst amount, dye concentration, and the NaBH<sub>4</sub> amount. Moreover, the GL/Co-SnO<sub>2</sub> nanocomposite catalyst can be easily recovered, is recyclable, and revealed minimal loss of nanomaterials.



**Citation:** Marwani, H.M.; Ahmad, S.; Rahman, M.M. Fabrication of 3D Gelatin Hydrogel Nanocomposite Impregnated Co-Doped SnO<sub>2</sub> Nanomaterial for the Catalytic Reduction of Environmental Pollutants. *Gels* **2022**, *8*, 479. <https://doi.org/10.3390/gels8080479>

Academic Editors: Chun Zhao and Takehiko Gotoh

Received: 22 June 2022

Accepted: 25 July 2022

Published: 29 July 2022

**Publisher's Note:** MDPI stays neutral with regard to jurisdictional claims in published maps and institutional affiliations.



**Copyright:** © 2022 by the authors. Licensee MDPI, Basel, Switzerland. This article is an open access article distributed under the terms and conditions of the Creative Commons Attribution (CC BY) license (<https://creativecommons.org/licenses/by/4.0/>).

**Keywords:** gelatin hydrogel; Co-SnO<sub>2</sub> nanomaterial; catalytic reduction; recyclability; environmental remediation

## 1. Introduction

Generally, polymers have been part of the lives of human beings from the beginning, because of their wide application in daily uses and unique properties. Due to their large-scale contribution in engineering resins, polyolefins, epoxies from tar to shellac, as well as tortoise, they provide basic and high-priority construction materials, transportation, commerce, and digestive products. Globally, polymers produce a large amount of money in the range of GBP 250–400 billion. Therefore, biopolymers, such as cellulose, chitins, lipids, proteins, and gelatin are an extensive part of the organic nature of sediments [1]. Biopolymer films are environmentally friendly and can be used in catalysis and food packaging [2–8]. Considering biopolymers, it reveals the feeble mechanical strength that limits their application in the catalyst field [9]. Gelatin is a biopolymer obtained from natural polymer collagen using hydrolysis. It is a flavorless, translucent, light yellowish, brittle, solid substance, derived under both acidic and basic conditions. Due to its universal properties, such as biocompatibility, cell-adhesion ability, modification, biodegradability,

and non-immunogenic properties, it is mostly used in cosmetic manufacturing, pharmaceuticals, photography, and gelling agents. Together with its readiness and inexpensiveness, gelatin is generally blended with other molecules and can be used extensively for drug delivery and engineering [10,11]. In contrast, in the physiological condition, the polymer possesses poor mechanical properties and short degradation time, and it can be difficult to shape it into a stable hydrogel gelatin with desirable mechanical properties [12]. To overcome this drawback, the addition of different fillers including metals, ceramics, air, and minerals can generate a unique hydrogel nanocomposite that exhibits competitive physical properties [13,14]. These incorporated materials enhance the functionality and flexibility, inherent to plastic, of the fabricated hydrogel nanocomposite. The term nanocomposite was first reported in the 1980s, which refers to the multicomponent system [15,16]. The major part is composed of a polymer and the minor part is composed of NPs that are at least one dimension below 100.0 nm. Polymer hydrogel nanocomposite is a synonym for inorganic–organic blended mixtures.

The first part of this blended mixture consists of a hydrogel (water + polymer). Hydrogels are soft interconnected natural/synthetic materials, that can swell several times, up to 99%, when absorbing and retaining a large quantity of water or other organic fluids, saline, and other physiological solutions in their three-dimensional (3D) structures. Hydrogels prevent dissolution of the structure [17–20]. They can be crosslinked via physical or chemical bonds [21,22]. Physically, they are crosslinked by noncovalent bonding, e.g., hydrogen bonding and van der Waals interaction, etc., while chemically hydrogels are crosslinked by adding different crosslinking agents, ultrasound, heating,  $\gamma$ -irradiation, or UV. Physical gels can be dissolved in water upon heating, while chemical gels are not dissolved in water [23]. They are extensively used for many industrial and medical purposes, such as solvent compositions, pH, temperature, cellular therapies, tissue engineering, stem-cell engineering, implants, and cancers [24–31]. The second part is composed of nanomaterials because, mechanically, hydrogels are fragile, weak, and brittle when they swell up, which limits their applications. Therefore, the incorporation of NPs enhanced the mechanical properties of prepared hydrogels [32,33]. The NPs absorb on the polymer chains when entrapped or crosslink the hydrogel network [22]. Often, the synthesized hydrogel and nanoparticles work synergistically and create optical, mechanical, and thermal properties in the combined blended form. These properties allow hydrogel nanocomposites to be used in sensors, separation devices, electronics, optics, and catalysts [34]. Gelatin has a water binding capacity due to hydroxyl (-OH), carboxylic (-COOH), and amino (-NH<sub>2</sub>) functional groups, which mainly participate in hydrogel formation. The common crosslinkers used for gelatin are bisvinyl sulfonemethyl (BVSM), genipin, citric acid, glutaraldehyde, 1,4-butanediol diglycidyl ether (BDDGE), and formaldehyde [35–41]. These crosslinkers target the above-mentioned functional groups. Luque et al. reported on the tin dioxide (SnO<sub>2</sub>) nanoparticles (NPs), which were synthesized by green synthesis, using different concentrations of orange-peel extract (*Citrus sinensis*) as a reducing agent. The SnO<sub>2</sub> NPs obtained were used for photocatalytic degradation of methylene blue (MB) [42].

In the present work, an efficient hydrogel nanocomposite is fabricated, incorporating Co-doped SnO<sub>2</sub> nanomaterials which are crosslinked within a gelatin matrix in the presence of formaldehyde as a crosslinker. The hydrogel nanocomposite material is further utilized for the catalytic reduction of different nitro-phenols as well as azo dyes for environmental and ecosystem safety on a broad scale.

## 2. Results and Discussion

### 2.1. FESEM and EDX

Figure 1 reveals the FESEM images of Co-SnO<sub>2</sub> nanomaterials and GL/Co-SnO<sub>2</sub> hydrogel nanocomposite materials. The fabricated nanomaterials were analyzed before and after crosslinking with the biopolymer. The first two images (Figure 1a,b) show the pure micrograph of Co-SnO<sub>2</sub> nanomaterial at low and high magnifications. Both images at low and high magnifications revealed the spherical shape of the nanomaterials. Further,

these magnified nanocomposite materials are presented in Figure 1b,b', respectively. In this case, the GL/Co-SnO<sub>2</sub> nanomaterials are crosslinked with formaldehyde via in situ formation, which remains firm within the hydrogel for long time and plays a vital role in the field of catalysis. This process is fit for entrapping NPs inside polymeric chains. It was observed that Co-SnO<sub>2</sub> nanomaterials are found in dispersed forms inside hydrogel networks. The SEM images clearly revealed that Co-SnO<sub>2</sub> nanomaterials are well dispersed inside the gelatin matrix. The average diameter of Co-SnO<sub>2</sub> is 17.5 nm in the range of 15–25 nm.

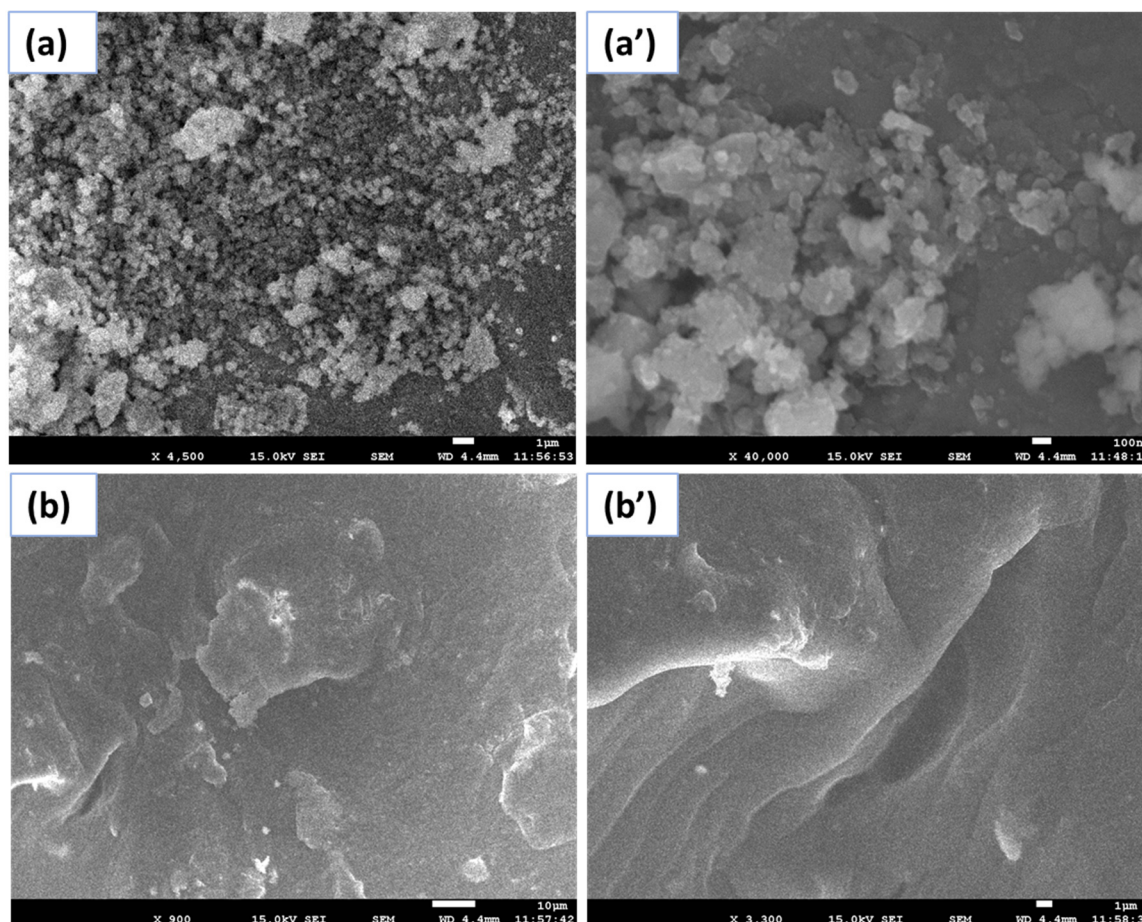


**Figure 1.** FESEM images of pure Co-SnO<sub>2</sub> nanomaterial (a) and GL/Co-SnO<sub>2</sub> nanocomposite material (b) of low and high magnification images (a',b'), respectively.

Here, the energy dispersive X-ray spectroscopy (EDX) method was utilized to analyze the elemental composition of the synthesized nanomaterial catalyst. The stoichiometry is shown in Figure 2. Oxygen (O), cobalt (Co), and tin (Sn) are the key elements of this prepared nanomaterial, while carbon contents appeared in the nanocomposite due to the involvement of the polymer. The EDX spectrum is displayed as 23.41%, 25.95%, and 55.00% by weight of Co, O, and Sn, respectively. This amount is decreased in GL/Co-SnO<sub>2</sub> nanocomposite material. The amount is reduced to 9.83% and 35.96% for Co and Sn, respectively. Before analysis, the sample was coated with GL, that is why the carbon peaks appeared as shown in the EDX spectra of the GL/Co-SnO<sub>2</sub> catalyst. Therefore, Figure 2b reveals the homogenous mixing of the Co-SnO<sub>2</sub> nanomaterial in the 3D-hydrogel network.

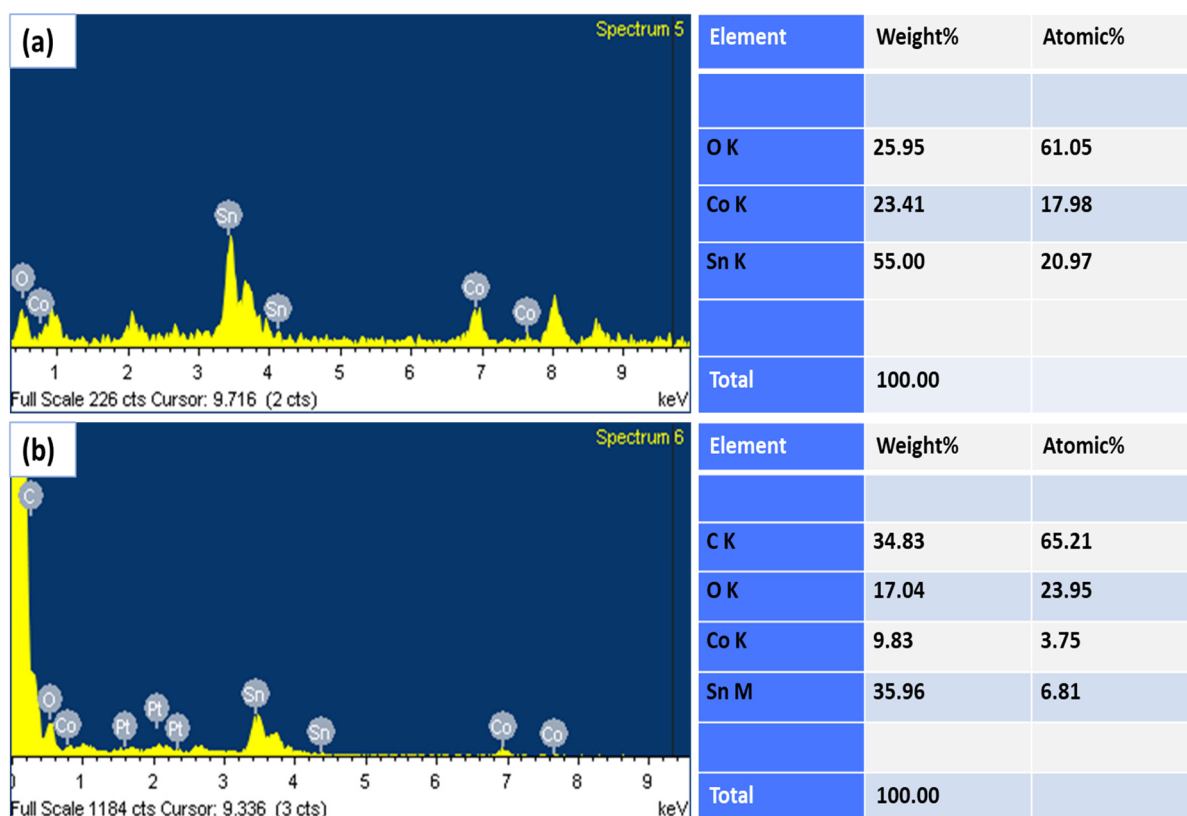


**Figure 2.** EDX spectra of Co-SnO<sub>2</sub> nanomaterial (a) and GL/Co-SnO<sub>2</sub> hydrogel nanocomposite material (b).

## 2.2. XRD

X-ray diffraction (XRD) was investigated to reveal the crystallinity of Co-doped SnO<sub>2</sub> and crosslinked Co-doped SnO<sub>2</sub> with GL. The XRD peaks for both Co-doped SnO<sub>2</sub> and GL/Co-doped SnO<sub>2</sub> hydrogel nanocomposite were obtained in the 2-theta range of 10–80° as shown in Figure 3. Pure Co-doped SnO<sub>2</sub> nanomaterial gives a 2 theta of 26.83°, 34.17°, 37.58°, 52.07°, 62.85°, 66.52°, and 79.37°. These crystalline peaks could be indexed to (110), (101), (200), (211), (310), (301), and (321). The crystalline diffraction peaks can be absolutely corresponding to tetragonal rutile SnO<sub>2</sub> (JCPDS card no. 41-1445) [43]. One additional peak appeared at 2 theta 37.58° which can be indexed to 200. This peak might be due to the Co-doped SnO<sub>2</sub> composite structure. The cobalt (Co)-doped oxide revealed a peak at 2 theta at 18.63°, 30.27°, 32.10°, 45.75°, and 57.68°, which could be indexed to (111), (220), (311), (400), and (511), respectively. Additionally, the high intensity peak that appeared at 32.10° could be indexed to (101) which could be corresponding to SnO<sub>2</sub>, which is in good agreement with the given literature [44–47]. These peaks are in good agreement with the JCPDS card no: 073-1701 file, which indicates the cubic structure of Co(NO<sub>3</sub>)<sub>2</sub>·6H<sub>2</sub>O [48]. The dry hydrogel nanocomposite material (GL/Co-doped SnO<sub>2</sub>) verifies two crystalline peaks at 34.17° and 52.07°, corresponding to (101) and (211), respectively. A broader peak was observed at 25.20°, which showed the amorphous form of the polymer. The fabricated nanocomposite shows no peaks in the catalyst that may be owing to the small quantity of cobalt oxide compared to the tin dioxide.

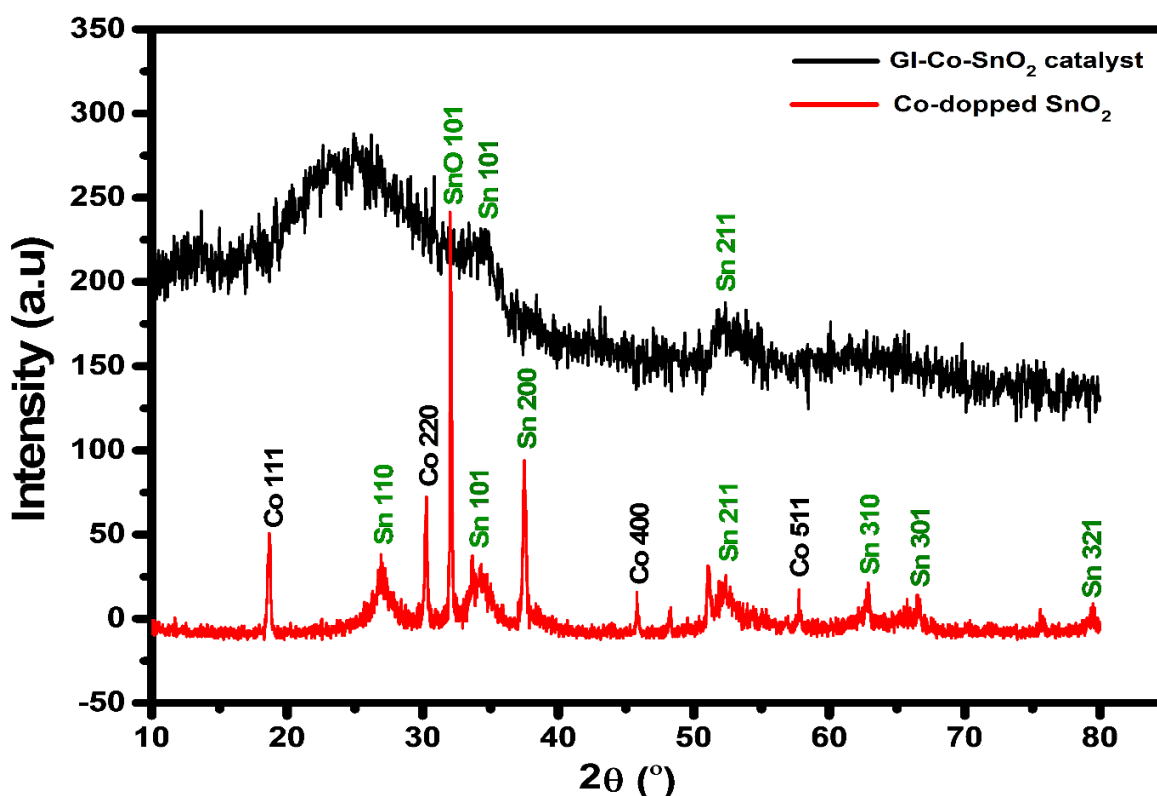


**Figure 3.** XRD patterns of Co-SnO<sub>2</sub> nanomaterial (dark line) and GL/Co-SnO<sub>2</sub> hydrogel nanocomposite material (red line).

The crystallinity of GL/Co-doped SnO<sub>2</sub> nanomaterial was calculated using Debye–Scherrer’s equation as follows.

$$D = \frac{k\lambda}{\beta \cos\theta} \quad (1)$$

In the above equation,  $D$  is the average diameter of the crystallites (nm),  $\lambda$  is the wavelength of CuK $\alpha$ 1 radiation (1.542 Å),  $\beta$  is the full width at half maximum in radians (FWHM), and  $\theta$  is the Bragg angle in the plane of the diffraction peak. The average crystalline diameter of the Co-doped SnO<sub>2</sub> nanomaterial was calculated as 10.19 nm.

### 2.3. ATR-IR

The composition of prepared NPs and fabricated nanocomposite catalyst was analyzed using ATR-IR spectroscopy, as shown in Figure 4. The ATR-IR spectrum of Co-SnO<sub>2</sub> nanomaterial shows their characteristic peaks at 1639 and 3371 cm<sup>-1</sup> which are attributed to OH bending, and OH stretching, respectively. The peak that appeared at a lower wavenumber corresponds to the stretching of the M–O (metal–oxygen stretching), which is in accordance with the given literature [49]. Further, the GL/Co-SnO<sub>2</sub> hydrogel nanocomposite provides stretching of the N–H functional group present in gelatin at 3270 cm<sup>-1</sup>. The peak that appeared in the nanocomposite at 1639 and 1539 cm<sup>-1</sup> presents amide I and asymmetric stretching vibration of the carboxyl group, respectively. Moreover, peaks located at 1452, 1404, and 1331 cm<sup>-1</sup> are attributed to C–H aliphatic vibration of the carboxyl group, C–H bending vibration, and stretching vibration of the C–N bond. In Figure 4b, the region from 475 to 510 cm<sup>-1</sup> is related to metal oxide, and hence confirms the presence of the prepared nanomaterial, i.e., gelatin-matrix/Co-SnO<sub>2</sub> nanomaterials.

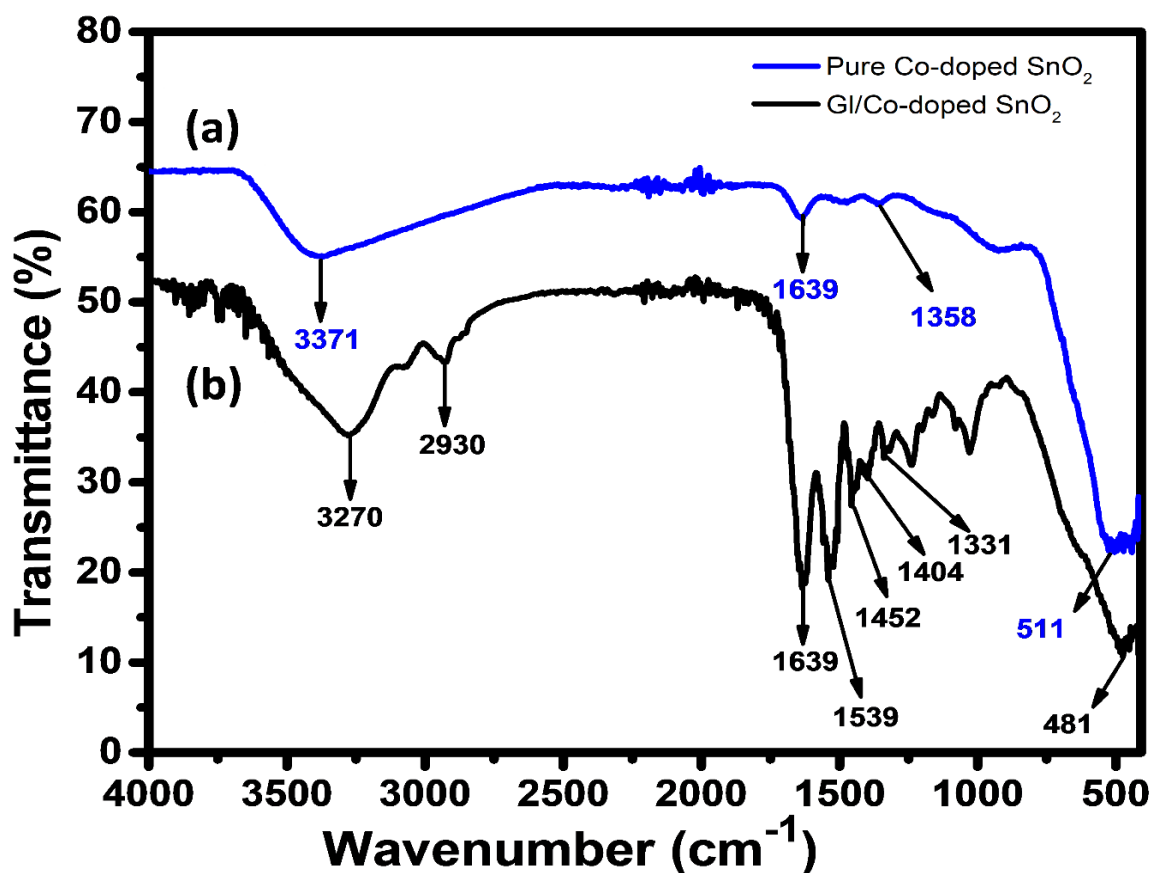


Figure 4. FTIR spectra of Co-SnO<sub>2</sub> nanomaterial (a) and GL/Co-SnO<sub>2</sub> hydrogel nanocomposite (b).

#### 2.4. Catalytic Reduction

The reduction of dyes was recorded using time-dependent absorbance with a UV-visible spectrometer from the 200–700 nm absorbance range, at room temperature. The reduction time for all the dyes was evaluated for 30 min. Moreover, the dye that took less time was used for further analysis. To study the effect of changing different parameters, such as different dosage of the catalyst, different concentrations of the dye and amounts of NaBH<sub>4</sub> were checked further against the dye. Additionally, at the end the major property of the catalyst, i.e., recyclability, was checked three times.

#### 2.5. Catalytic Reduction of GL/Co-SnO<sub>2</sub> Nanocomposite Material

Hydrogel is a hydrophilic polymer, which is crosslinked by chemical or physical interactions containing a large amount of water [50–56]. It swells in the aqueous solution by absorbing water in its three-dimensional network. Therefore, the dye molecules can easily filter through it. Herein, the prepared GL/Co-SnO<sub>2</sub> was used against nanomaterial and chemical/azo dyes. The nitro groups containing compounds are widely implemented in pharmacology goods, dyes, and pigment industries, and aromatic products for colored dye [57]. For example, analgesic as well as antipyretic medicines (Acetanilide, Paracetamol, and Phenacetin) are synthesized in industries from 4-amino-phenol that can be acquired through catalytic-reduction of 4-NP [58,59]. Additionally, the products obtained from 2-NP and 2,6-DNP are mostly used as herbicides and dye pigments, respectively. Besides their importance, they also pollute the ecosystem due to their toxic nature, being released from various industries. Thus, their catalytic reduction is important to reduce their toxicity and convert them into safer products. Therefore, catalytic reduction is a significant process for the reduction of these pollutants. With the catalytic reduction, 4-NP, 2-NP, and 2,6-DNP were transferred into their corresponding amines and the reduction process was monitored with UV-vis. spectroscopy by using the uninterrupted decline in spectra. Thermodynami-

cally, these proposed reactions are reasonable in the aqueous phase of the reducing agent ( $\text{NaBH}_4$ ). Significant changes between dye compounds and a good reducing agent ( $\text{NaBH}_4$ ) generates a large kinetic barrier, which reduces the reduction at very slow rate even with a large quantity of reducing agent ( $\text{NaBH}_4$ ) [60–65]. By introducing an efficient catalyst, it exceeds this energy barrier and allows the catalytic reaction to occur.

Herein, the 2-NP, 2,6-DNP, and 4-NP were investigated with a strong reducing agent, i.e.,  $\text{NaBH}_4$ , which did not show considerable reduction even after a long time. While, the experiment was repeated by introducing the fabricated catalyst, i.e., Co-doped  $\text{SnO}_2$ , and reduced all dyes within 30 min. For the catalytic reduction of nitro aromatic compounds, such as 2-NP, 2,6-DNP, and 4-NP, 25.0 mL of each pollutant was used with a strong reducing agent ( $\text{NaBH}_4$ ) and 0.2 gm hydrogel nanocomposite. The catalyst facilitates hastening of electron transfer from donor  $\text{BH}_4^-$  to the acceptor, nitro-compounds, and the reduction of the reaction proceeds [66]. The catalytic reduction was carried out by tracking the decrease in the absorbance peak in different time intervals, which is presented in Figure 5a–c. The catalytic reduction was carried out in the excess of  $\text{NaBH}_4$ . The reaction was supposed to follow the first-order reaction condition. Therefore, to calculate the apparent rate constant ( $K_{\text{app}}$ ) of nitro aromatic compounds, pseudo-first-order kinetics were used. The slope of the straight line provides the magnitude for apparent rate constant plotted between  $\ln(C_t/C_0)$  against time. The reduction process was investigated using the following pseudo-first-order equation.

$$\ln(C_t/C_0) = \ln(A_t/A_0) = -K_{\text{app}} t \quad (2)$$

where  $C_0$  and  $C_t$  are the initial concentration and final concentration of the dye at any given interval of time.  $A_0$  is the absorbance of the dye at the start and  $A_t$  is the absorbance value taken after introducing  $\text{NaBH}_4$  and catalyst to the reaction media.  $K_{\text{app}}$  represents the apparent rate constant, while ' $t$ ' represents the rate of the reaction.

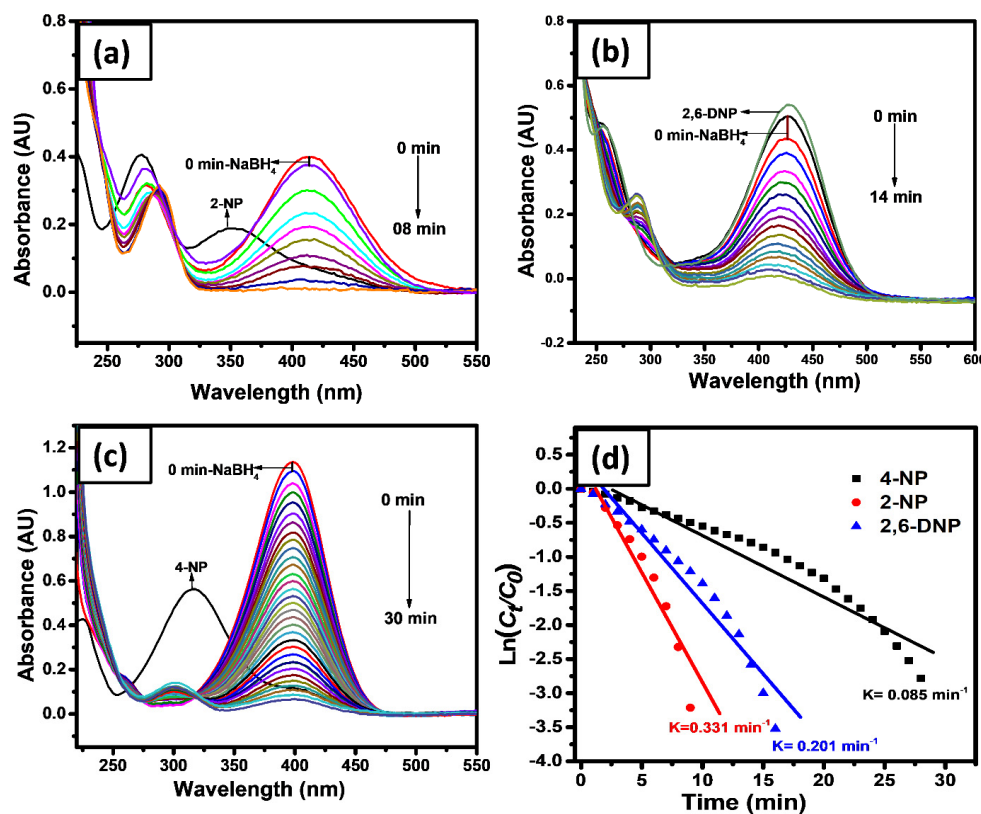


**Figure 5.** Typical UV-visible absorbance spectra of 2-NP (a), 2,6-DNP (b), and 4-NP (c) and their  $\ln(A_t/A_0)$  vs. time plot for the reduction reactions where the amount of the GL/Co- $\text{SnO}_2$  catalyst used was 0.2 gm (d).

The % reduction of the dyes was expressed using Equation (2).

$$(\%) C/C_0 = [(A_0 - A_t)/A_0] \times 100 \quad (3)$$

where  $A_0$  and  $A_t$  correspond to the initial absorbance of the dye '0 min' and absorbance at time ' $t$ ', respectively.

The reduction reactions were performed in a beaker by introducing 25.0 mL of each nitrophenol (2-NP, 2,6-DNP, and 4-NP), 0.4 gm of  $\text{NaBH}_4$ . A fixed concentration of 0.07 mM of the dye was used for each run. The catalytic reduction was initiated by introducing 0.2 gm of  $\text{Co-SnO}_2$  photocatalyst. The UV-vis spectrum of the 2-NP, 2,6-DNP, and 4-NP exhibits absorption peaks at 412, 426, and 397 nm, respectively. The nitrophenols were reduced in 8, 14, and 30 min, respectively. Additionally, the catalytic reduction rate of the reaction was reported as  $3.31 \times 10^{-1}$ ,  $2.01 \times 10^{-1}$ , and  $8.9 \times 10^{-2} \text{ min}^{-1}$ , respectively. Among which, the reduction rate for 4-NP was very slow. The catalytic reduction rate,  $K_{\text{app}}$ , of nitrophenols between  $\ln(C_t/C_0)$  verses time are shown in Figure 5d.

### 2.6. Catalytic Reduction of Azo Dyes

The photocatalytic reduction of azo dyes (CR and MO) was studied with an excess amount of  $\text{NaBH}_4$  (model reaction), which are presented in Figure 6a–d. The  $\text{NaBH}_4$  acts as an electron source for the reduction of dye molecules. Generally, the borohydride ion and dye molecule adsorb simultaneously on the surface of NPs, where the transfer of electrons takes place from  $\text{BH}_4^-$  to the surface of the  $\text{GL/Co-SnO}_2$  nanomaterial, which transfers it to dye molecules and reduces it. Here, we fabricated  $\text{GL/Co-SnO}_2$  and used it for reduction of CR and MO with ( $\lambda_{\text{max}}$ ) at 475 and 461 nm, respectively. The same condition was used for the reduction of the dyes, as discussed above. With the addition of  $\text{NaBH}_4$  it did not cause fading, while slightly decreased the intensity of its color. The introduction of hydrogel nanocomposite to the aqueous media containing dye and  $\text{NaBH}_4$  starts the reduction of the dye molecules. The catalyst acts as an electron relay system, it takes the electron from the donor  $\text{BH}_4^-$  and conveys it to the dyes [67]. The UV spectrum illustrates the two broad peaks of CR and MO, owing to the presence of the  $-\text{N}=\text{N}-$  double bond. The CR and MO were reduced in 5 and 3 min, respectively. The photocatalytic reduction rate constants of these dyes were reported (Figure 6c,d) as  $6.61 \times 10^{-1}$  and  $1.036 \text{ min}^{-1}$ , respectively. The MO reduction rate was higher than CR. As MO is one of the persistent and toxic dyes its catalytic reduction was studied further in detail.

The effect of catalyst dosage was also investigated against MO, keeping other parameters constant. Three different hydrogel nanocomposites ( $\text{Co-SnO}_2$ ), i.e., 0.1, 0.2, and 0.4 gm were analyzed against 0.07 mM of MO with 0.4 g of  $\text{NaBH}_4$ . The reduction rate was calculated as 0.713, 1.036, and  $2.287 \text{ min}^{-1}$ , respectively. Compared to the amount of the catalyst, it showed a direct effect on the catalytic reduction of the dye (Figure 7a). For example, MO was reduced in 04, 03, and 02 min, respectively. The  $K_{\text{app}}$  value for the catalytic reduction of MO with the hydrogel nanocomposite was calculated from the slope of the linear line plotted between  $\ln(C_t/C_0)$  verses time, as shown in Figure 7b.

The optimization of the effect of different amounts of catalytic reducing agents ( $\text{NaBH}_4$ ) on the catalytic reduction rate of the MO was examined. By increasing the amount of  $\text{NaBH}_4$  the reduction rate,  $K_{\text{app}}$ , increased, as can be seen from the slope between  $\ln(C_t/C_0)$  verses time in Figure 7c. Three different weights of 0.2, 0.4, and 0.8 gm of  $\text{NaBH}_4$  were added to the MO. The 25.0 mL of 0.07 mM MO was reduced in 05, 02, and 01 min, respectively. The rate of the reduction was recorded as 0.722, 1.036, and  $3.033 \text{ min}^{-1}$ , respectively. The increase in the amount of  $\text{NaBH}_4$  has a positive effect on the efficient reduction rate of the fabricated catalyst. This is due to the availability of more  $\text{BH}_4^-$  ions. The reason is that these electron-rich species accelerate quickly in the reaction phase and as a result promptly provide electrons towards hydrogel nanocomposites which convey them to the dye molecules.

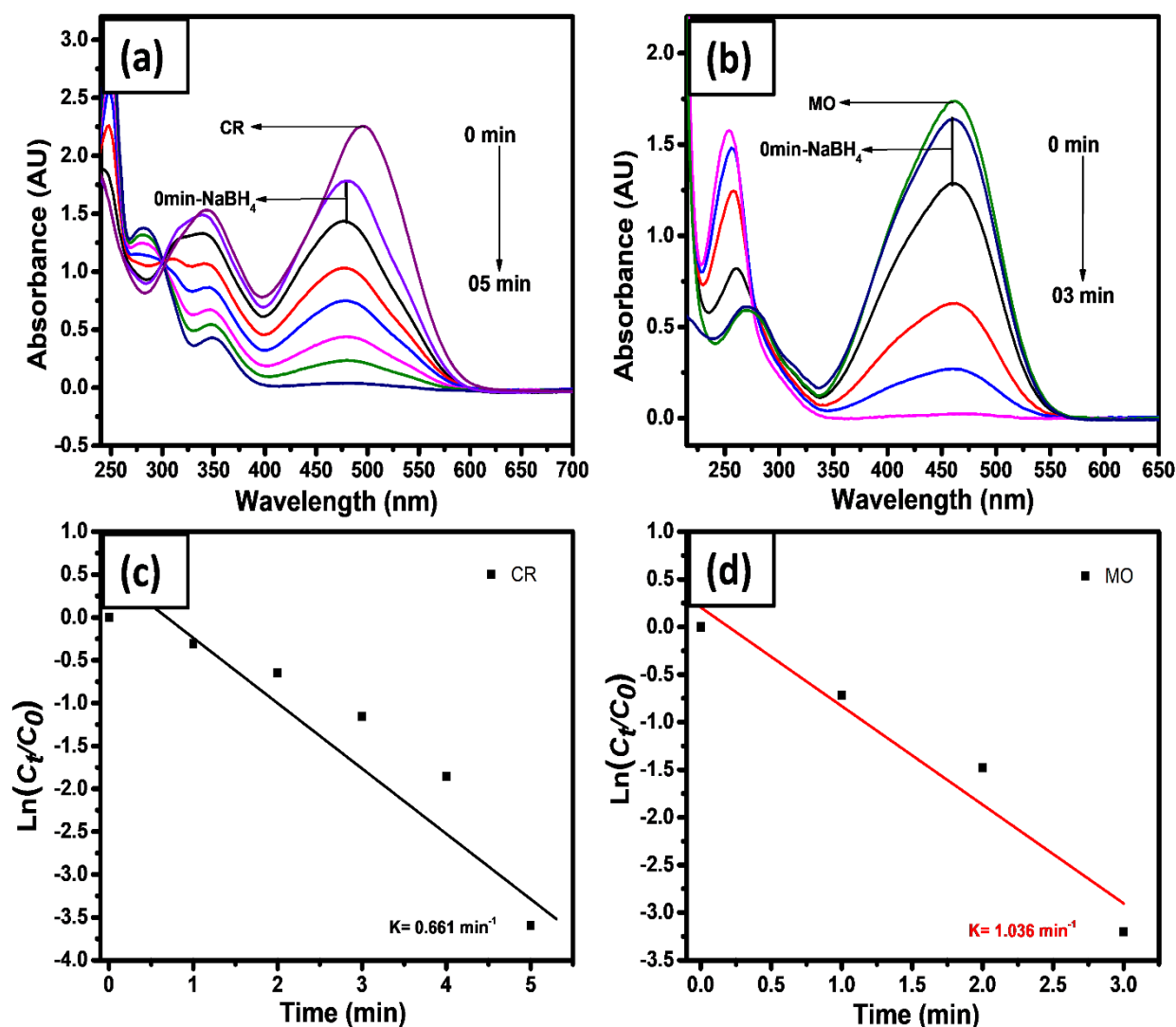


**Figure 6.** Typical UV-visible absorbance spectra of CR (a), MO (b), and their and  $\ln(A_t/A_0)$  vs. time plot for the reduction reactions (c,d), where 0.2 gm of the amount of the GL/Co-SnO<sub>2</sub> catalyst was used respectively.

To analyze the photocatalytic reduction of Co-doped SnO<sub>2</sub> catalyst for different concentrations of MO, three different concentrations of MO were prepared, such as 0.05, 0.07, and 0.09 mM, keeping other parameters constant. Figure 7d clearly illustrates that with the increase in concentration of the dye, it took more time to be reduced. Therefore, MO with the above concentration was reduced in 02, 03, and 04 min, respectively. Finally, it is understood from the experimental results that the catalytic reaction rate of the reaction increases by decreasing the concentration of the colored dye. Then, the reaction rate was reported as 1.656, 1.036, and 0.921 min<sup>-1</sup>, respectively. The reduction of all dyes gives a linear straight line between  $\ln(C_t/C_0)$  versus time followed by pseudo-first-order reaction. Then, the rate constant  $K_{app}$  of the reaction was calculated using equation 1. Thus, the catalytic efficiency of the hydrogel nanocomposite showed a direct effect with the amount of NaBH<sub>4</sub>, concentration of MO dye, and the amount of catalyst, as illustrated in Figure 7a–d.

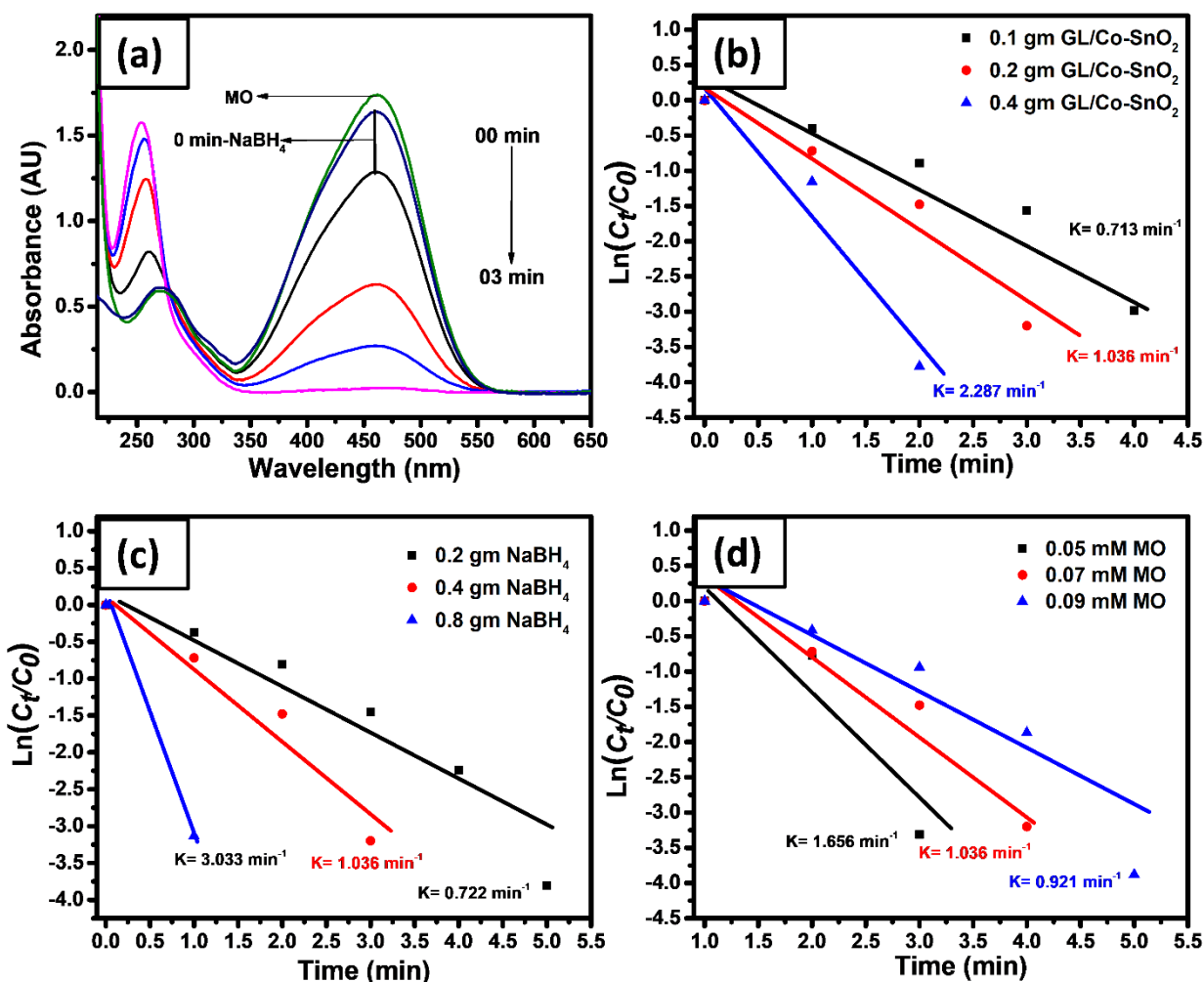


**Figure 7.** UV-visible spectra of MO reduction (a) and the plot of  $\ln(C_t/C_0)$  versus time for CR by changing the amount of GL/Co-SnO<sub>2</sub> catalyst, (b) changing the amount of  $\text{NaBH}_4$ , (c) and different concentrations of dye (d).

### 2.7. Recyclability

In this approach, one of the challenging properties of the catalyst is its recyclability because this property reduces the re-scale operations, costs, and economic value. In this case, after completion of the reaction, the catalyst is recovered simply by filtration. It is washed three times with distilled water before using it for the next cycle. Herein, the catalyst was consecutively recycled three times. Figure 8 showed that 25.0 mL of the 0.07 mM of dye was reduced in 03, 05, and 07 min, with the reduction rates of 1.036, 0.616, and 0.455  $\text{min}^{-1}$ , respectively. The dye was reduced nearly up to 97.67, 96.99, and 96.88%, respectively. In each cycle, there is a small loss of effectiveness of nanocomposites. In Figure 8,  $(C/C_0)$  % shows the percentage of reduction in each cycle, while Kapp represents the apparent rate constant on the right-hand side of the bar graph. It is evident that the percentage of the reaction is almost the same, while the rate of the reaction changes with time.

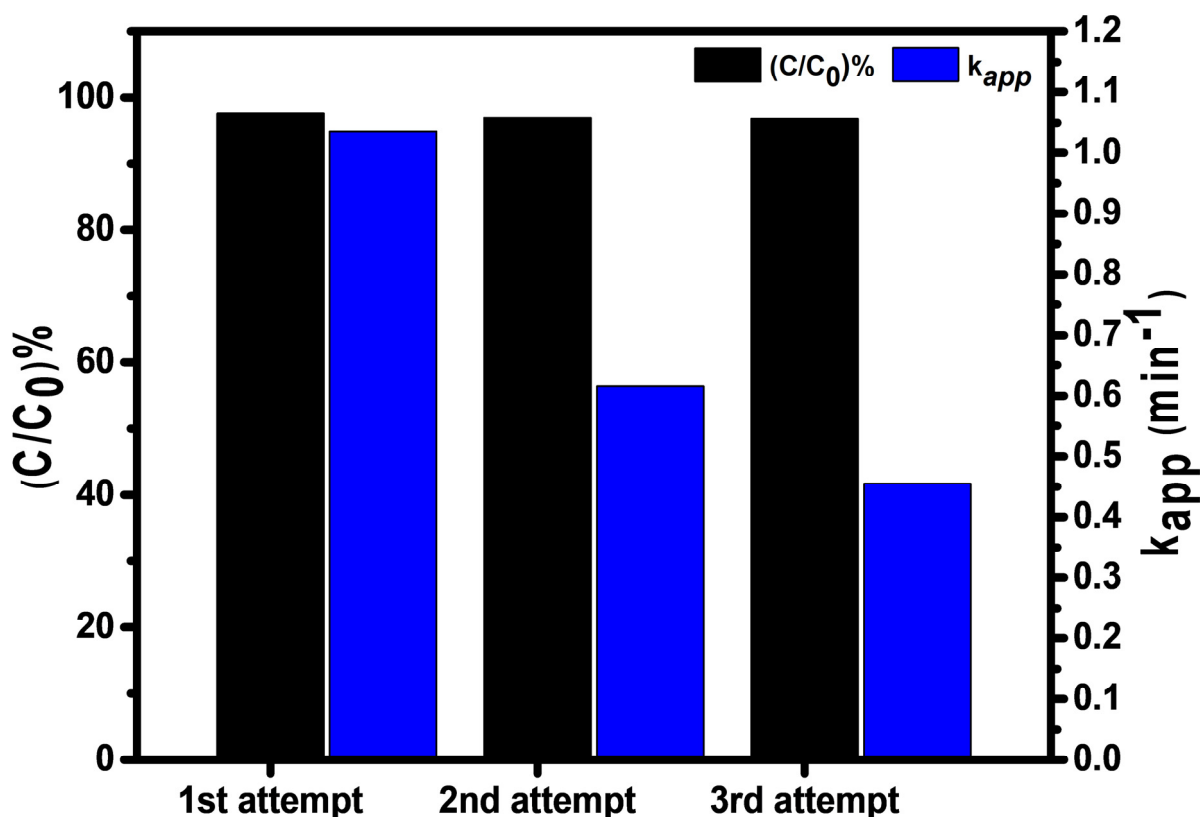
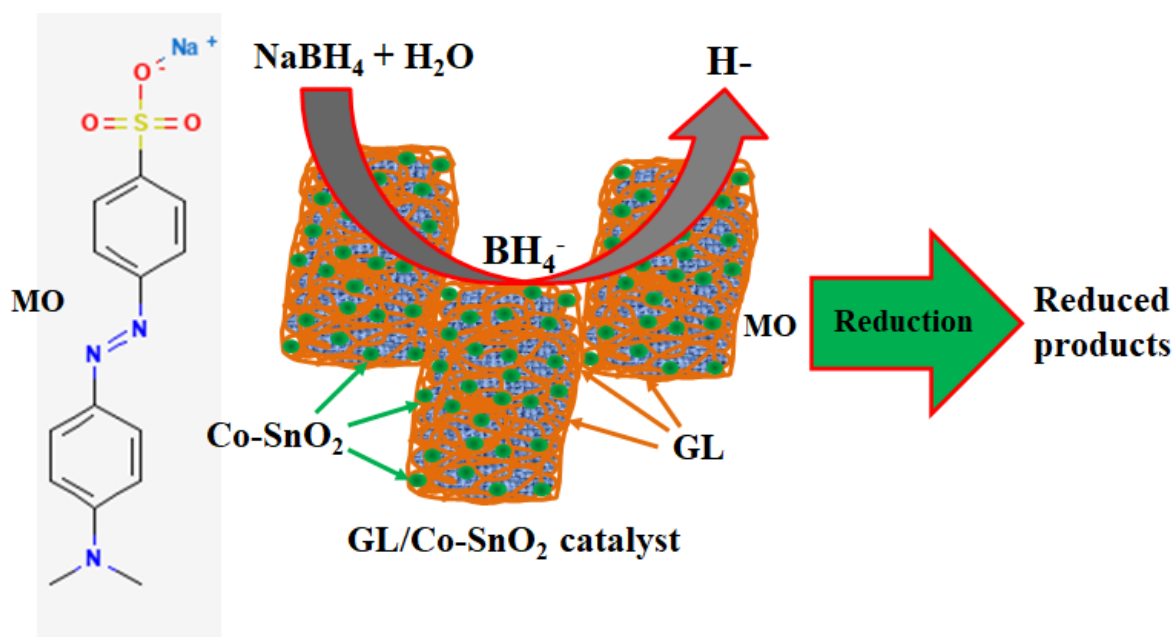


Figure 8. Recyclability of the GL/Co-SnO<sub>2</sub> nanocomposite catalyst.

### 2.8. Mechanism of Reduction

MO is a water-soluble azo dye widely utilized in various dyes and pigment industries. Besides the importance of this dye in terms of application, it is also unsafe and carcinogenic in nature. Therefore, from the environmental and ecological points of view, MO's reduction is very important and significant. Catalytic reduction of the MO cannot be supported by the reducing agent (NaBH<sub>4</sub>) because the reaction kinetics are not viable. Therefore, in this approach, the reduction of MO molecules was carried out in the presence of the GL/Co-SnO<sub>2</sub> nanocomposite catalyst with the reducing agent, NaBH<sub>4</sub>. Here, Figure 9 exhibits the catalytic reduction of MO molecules, that are converted into their corresponding small constituents of MO. After introducing the GL/Co-SnO<sub>2</sub> catalyst into the reactors, the higher concentration of sodium borohydride was implemented to the aqueous solution of MO, that increased the pH of the resultant solution mixture. In this catalytic process, the reducing agent gives BH<sub>4</sub><sup>-</sup> which acts as an electron donor in the system. In the presence of the prepared GL/Co-SnO<sub>2</sub> catalyst, the BH<sub>4</sub><sup>-</sup> and MO dye molecules are adsorbed onto the surface of the GL/Co-SnO<sub>2</sub> catalyst. The surface of the GL/Co-SnO<sub>2</sub> nanomaterial acts as mediator for transferring electrons from the BH<sub>4</sub><sup>-</sup> ion towards MO dye molecules. The GL/Co-SnO<sub>2</sub> catalyst introduces an efficient pathway to transfer electrons to the MO dye molecules, which reduced it in a short amount of time. Finally, the MO dye molecule was converted into small constituents.



**Figure 9.** Catalytic reduction of MO in the presence of NaBH<sub>4</sub> onto the GL/Co-SnO<sub>2</sub> nanocomposite catalyst.

### 3. Conclusions

In this experimental procedure, we fabricated Co/Sn nanomaterial using a facile and one-step mechanism known as the co-precipitation method. The Co-SnO<sub>2</sub> catalyst nanomaterial was simply prepared by direct mixing of SnCl<sub>2</sub>·2H<sub>2</sub>O and Co(NO<sub>3</sub>)<sub>2</sub>·6H<sub>2</sub>O at high pH > 10. The nanomaterials with an average diameter size of 10.19 nm were dispersed in the viscous solution of the GL polymer and crosslinked chemically using formaldehyde. In order to easily recover them from the reaction media and prevent them from aggregation, these nanomaterials were crosslinked with the GL polymer. Additionally, owing to the presence of a large number of functional groups on the main chain of the GL polymer, such as -OH, -COOH helps with packing nanomaterial inside the polymer chains. The prepared nanocomposite was investigated for the reduction of different chemicals and dyes (2-NP, 2,6-DNP, 4-NP, CR, and MO). The catalytic reduction rate of the reaction followed the order, MO > CR > 4-NP > 2,6-DNP > 2-NP. Among which, MO was reduced efficiently with a strong reducing agent (NaBH<sub>4</sub>) with a reduction rate of 1.036 min<sup>-1</sup>. MO was further studied in detail changing different parameters. The catalytic efficiency of the GL/Co-SnO<sub>2</sub> was very significant due to the production of H<sub>2</sub> gas, which kept the surface clean for the coming dye molecules. It introduced a new route for the mineralization of unsafe chemicals and colored dyes using the reduction method with newly introduced GL/Co-SnO<sub>2</sub> nanocomposite materials for the safety in environmental and ecological fields on a broad scale.

### 4. Experimental Section

#### 4.1. Materials and Methods

In this section, chemicals and reagents used in this study were of analytical grade without further purification. Cobalt (II) nitrate hexahydrate [Co(NO<sub>3</sub>)<sub>2</sub>·6H<sub>2</sub>O; 98%], tin (II) chloride dihydrate (SnCl<sub>2</sub>·2H<sub>2</sub>O; 98%), Congo red (C<sub>32</sub>H<sub>22</sub>N<sub>6</sub>Na<sub>2</sub>O<sub>6</sub>S<sub>2</sub>), and methyl orange (C<sub>14</sub>H<sub>14</sub>N<sub>3</sub>NaO<sub>3</sub>S) were from the Sigma-Aldrich chemical company (St. Louis, MO, USA). Gelatin hydrogel (C<sub>102</sub>H<sub>151</sub>O<sub>39</sub>N<sub>31</sub>), 4-nitro-phenol (4-NP; C<sub>6</sub>H<sub>5</sub>NO<sub>2</sub>; 97%), 2-nitro-phenol (2-NP; C<sub>6</sub>H<sub>5</sub>NO<sub>2</sub>; 98.5%), and 2,6-dinitro-phenol (2,6-DNP; C<sub>6</sub>H<sub>4</sub>N<sub>2</sub>O<sub>5</sub>; 99.9%) were purchased from Fluka (London, UK). Sodium borohydride (NaBH<sub>4</sub>, 97%) was purchased

from BDH chemicals (London, UK) and used without further purification. Double distilled water was utilized to make all chemical and material solutions for this analysis.

#### 4.2. Preparation of Co-Doped SnO<sub>2</sub> Nanomaterial with Hydrogel Nanocomposite

In this approach, Co-doped SnO<sub>2</sub> nanocomposite was synthesized using the co-precipitation method, which is presented in the Figure 10. Firstly, 50.0 mL of two salt solutions of SnCl<sub>2</sub>·2H<sub>2</sub>O of 0.1 M and Co(NO<sub>3</sub>)<sub>2</sub>·6H<sub>2</sub>O of 0.1 M were prepared in distilled water, respectively. In the second step, total volume of the solution of SnCl<sub>2</sub>·2H<sub>2</sub>O was discharged into 50.0 mL of Co(NO<sub>3</sub>)<sub>2</sub>·6H<sub>2</sub>O solution, which made the total volume of the solution 100.0 mL, while the pH of the solution was adjusted to 10 by slowly adding 0.2 M solution of NaOH. The homogenous mixture of solution was vigorously stirred. Further, the solution was heated at 70.0 °C under constant stirring for 24 h. Then, the resultant solution was cooled at room temperature and the black precipitate (pellet) was separated at 6000 rpm. The supernatant solution remaining above the pellet was discarded and the obtained precipitate was washed three times with distilled water. The prepared sample in powder-form was dried at 60 °C and stored in a plastic vial when not in use.

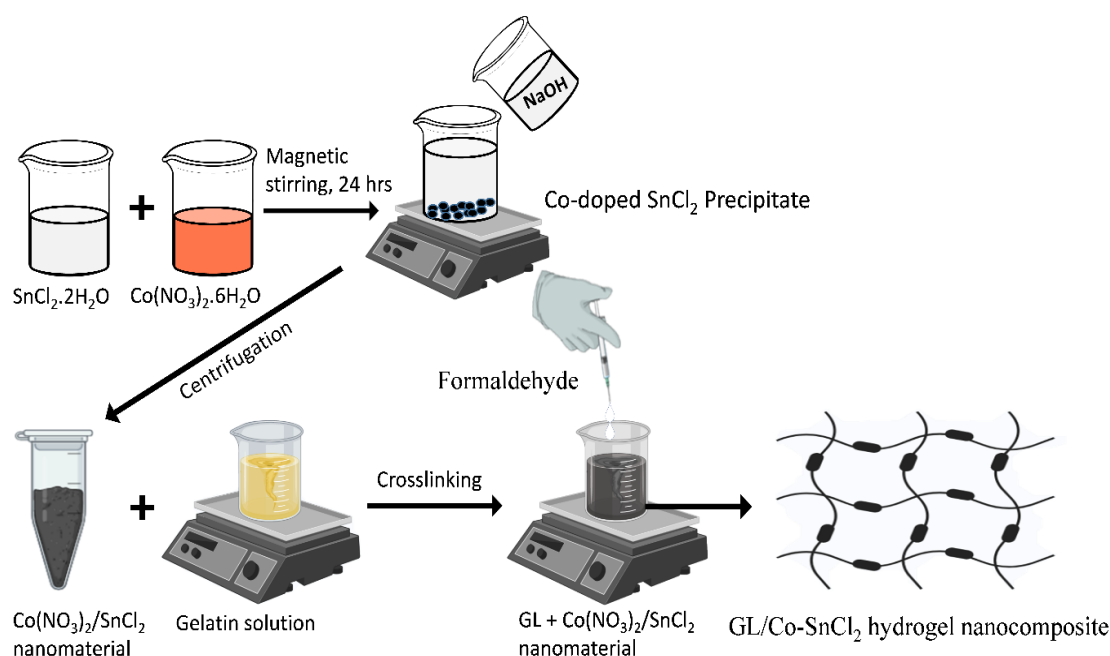


**Figure 10.** Preparation of GL/Co-SnO<sub>2</sub> hydrogel nanocomposite materials.

Further, the hydrogel was prepared by dissolving 0.24 gm of gelatin in enough water to make 30 mL of hydrogel solution. The solution was stirred for 40 min continuously. Further, 4% of 0.8 gm of the prepared nanomaterials (i.e., Co-doped SnO<sub>2</sub>) was mixed with 30 mL of gelatin aqueous solution. This mixture of hydrogel and nanomaterial was kept stirring for 25 min, to completely impregnate the Co-doped SnO<sub>2</sub> nanomaterials in the gelatin matrix. To crosslink these nanomaterials within gelatin polymer, a crosslinker formaldehyde was added dropwise with a syringe. Within a few minutes, the solution stopped stirring and a semi-solid structure was formed. This was kept overnight at room temperature for complete hydrogel formation.

#### 4.3. Catalytic Performance of Co-Doped SnO<sub>2</sub> Nanocomposite

In this experimental work, a fixed amount of 0.2 gm fabricated hydrogel nanocomposite, as a catalyst (GL/Co-SnO<sub>2</sub>), was added to 25.0 mL of each dye, such as 2-NP, 2,6-DNP, 4-NP, and CR, as well as MO, while 0.4 gm of NaBH<sub>4</sub> was added before the catalyst. The catalytic performance of Co-doped SnO<sub>2</sub> nanocomposite was checked against different nanomaterials and azo dyes. Five different chemical and dyes, such as 4-NP, 2-NP, 2,6-

DNP, CR, and MO were analyzed in the presence of fabricated catalyst, to investigate its catalytic efficiency. An aqueous solution of 0.07 mM was prepared for all these chemicals and dyes, using 0.2 gm hydro-gel nanocomposite as well as 0.4 gm NaBH<sub>4</sub>. All reactions were carried out under constant stirring. For spectral analysis of dyes, 5.0 mL of the syringe was half-filled with dye solution and poured into a quartz cell. The solution in the cuvette was poured into the beaker solution. This process was repeated until the dye reduced completely.

#### 4.4. Characterizations

For the morphology of Co-doped SnO<sub>2</sub> hydrogel nanocomposite material, field-emission scanning electron microscopy (FESEM) was performed with the JEOL instrument (JSM-7600F, Tokyo, Japan) at an accelerating voltage of 5.0 KV (magnification: ×40,000 Max). Before analysis of prepared samples, the dried sample was coated onto platinum, and a 1.5 cm-diameter cut was made with sticky black tape. The elemental composition of the prepared nanocomposite was analyzed using Oxford energy dispersive X-ray spectroscopy (EDX) equipment, which was connected directly with the FESEM instrument. Field-emission scanning electron microscopy (FESEM) is an instrumental technique utilized for the morphology of the prepared sample. A high energy beam is focused on the surface of the specimen to obtain the external morphology of the materials. Herein, the 3D hydrogel nanocomposite was dried at room temperature and investigated with FESEM. Crystallinity of the prepared sample was further investigated with powder X-ray diffraction (XRD) by using a PANalytical diffractometer with a K $\alpha$  radiation ( $\lambda = 0.154$  nm) source. The apparatus current of 50.0 mA and voltage of 40.0 KV were set for the investigation. The data was recorded in the range of 10–80° at a scan rate of 2° 2 $\theta$  min<sup>-1</sup>. Attenuated total reflection–Fourier transform infrared (ATR-FTIR) was used to characterize different functional groups in the Co-doped SnO<sub>2</sub> nanocomposite hydrogel. The spectra were recorded in the range of 40,000 to 500 cm<sup>-1</sup> during 64 scans using FTIR.

**Author Contributions:** Conceptualization, H.M.M. and S.A.; methodology, S.A.; software, S.A.; validation, S.A., H.M.M. and M.M.R.; formal analysis, S.A.; investigation, S.A.; resources, H.M.M.; data curation, S.A. and M.M.R.; writing—original draft preparation, S.A. and H.M.M.; writing—review and editing, M.M.R.; visualization, H.M.M. and M.M.R.; supervision, H.M.M.; project administration, H.M.M.; funding acquisition, H.M.M. All authors have read and agreed to the published version of the manuscript.

**Funding:** This work was funded by the Deanship of Scientific Research (DSR), King Abdulaziz University, Jeddah, under grant No. 130-54-D1443.

**Institutional Review Board Statement:** Not applicable.

**Informed Consent Statement:** Not applicable.

**Data Availability Statement:** Data will be available upon reasonable request.

**Acknowledgments:** This work was funded by the Deanship of Scientific Research (DSR), King Abdulaziz University, Jeddah, under grant No. 130-54-D1443. The authors, therefore, acknowledge with thanks DSR technical and financial support.

**Conflicts of Interest:** The authors declare no conflict of interest.

## References

1. Sorption of Organic Contaminants by Biopolymers: Role of Polarity, Structure and Domain Spatial Arrangement. Available online: <https://www.ncbi.nlm.nih.gov/pubmed/17095043> (accessed on 13 February 2020).
2. Khan, S.B.; Ali, F.; Kamal, T.; Anwar, Y.; Asiri, A.M.; Seo, J. CuO embedded chitosan spheres as antibacterial adsorbent for dyes. *Int. J. Biol. Macromol.* **2016**, *88*, 113–119. [[CrossRef](#)] [[PubMed](#)]
3. Bae, H.J.; Park, H.J.; Hong, S.I.; Byun, Y.J.; Darby, D.O.; Kimmel, R.M.; Whiteside, W.S. Effect of clay content, homogenization RPM, pH, and ultrasonication on mechanical and barrier properties of fish gelatin/montmorillonite nanocomposite films. *LWT Food Sci. Technol.* **2009**, *42*, 1179–1186. [[CrossRef](#)]

4. Kamal, T.; Ahmad, I.; Khan, S.B.; Asiri, A.M. Bacterial cellulose as support for biopolymer stabilized catalytic cobalt nanoparticles. *Int. J. Biol. Macromol.* **2019**, *135*, 1162–1170. [[CrossRef](#)]
5. Kamal, T.; Ul-Islam, M.; Khan, S.B.; Asiri, A.M. Adsorption and photocatalyst assisted dye removal and bactericidal performance of ZnO/chitosan coating layer. *Int. J. Biol. Macromol.* **2015**, *81*, 584–590. [[CrossRef](#)]
6. Ali, N.; Kamal, T.; Ul-Islam, M.; Khan, A.; Shah, S.J.; Zada, A. Chitosan-coated cotton cloth supported copper nanoparticles for toxic dye reduction. *Int. J. Biol. Macromol.* **2018**, *111*, 832–838. [[CrossRef](#)]
7. Ali, F.; Khan, S.B.; Kamal, T.; Alamry, K.A.; Asiri, A.M. Chitosan-titanium oxide fibers supported zero-valent nanoparticles: Highly efficient and easily retrievable catalyst for the removal of organic pollutants. *Sci. Rep.* **2018**, *8*, 6260. [[CrossRef](#)]
8. Ali, F.; Khan, S.B.; Kamal, T.; Alamry, K.A.; Asiri, A.M.; Sobahi, T.R.A. Chitosan coated cotton cloth supported zero-valent nanoparticles: Simple but economically viable, efficient and easily retrievable catalysts. *Sci. Rep.* **2017**, *7*, 16957. [[CrossRef](#)] [[PubMed](#)]
9. Lagoa, R.; Rodrigues, J.R. Kinetic analysis of metal uptake by dry and gel alginate particles. *Biochem. Eng. J.* **2009**, *46*, 320–326. [[CrossRef](#)]
10. Yuan, S.; Xiong, G.; Roguin, A.; Choong, C. Immobilization of gelatin onto poly (glycidyl methacrylate)-grafted polycaprolactone substrates for improved cell–material interactions. *Biointerphases* **2012**, *7*, 30. [[CrossRef](#)]
11. Echave, M.C.; Burgo, L.S.; Pedraz, J.L.; Orive, G. Gelatin as biomaterial for tissue engineering. *Curr. Pharm. Des.* **2017**, *23*, 3567–3584. [[CrossRef](#)]
12. Li, X.; Zhang, J.; Kawazoe, N.; Chen, G. Fabrication of highly crosslinked gelatin hydrogel and its influence on chondrocyte proliferation and phenotype. *Polymers* **2017**, *9*, 309. [[CrossRef](#)]
13. Al-Mubaddel, F.S.; Haider, S.; Aijaz, M.O.; Haider, A.; Kamal, T.; Almasry, W.A.; Javid, M.; Khan, S.U.-D. Preparation of the chitosan/polyacrylonitrile semi-IPN hydrogel via glutaraldehyde vapors for the removal of Rhodamine B dye. *Polym. Bull.* **2017**, *74*, 1535–1551. [[CrossRef](#)]
14. Ali, N.; Ismail, M.; Khan, A.; Khan, H.; Haider, S.; Kamal, T. Spectrophotometric methods for the determination of urea in real samples using silver nanoparticles by standard addition and 2nd order derivative methods. *Spectroc. Acta Pt. A-Molec. Biomolec. Spectr.* **2018**, *189*, 110–115. [[CrossRef](#)]
15. Fukushima, Y.; Inagaki, S. Synthesis of an intercalated compound of montmorillonite and 6-polyamide. In *Inclusion Phenomena in Inorganic, Organic, and Organometallic Hosts*; Springer: Berlin/Heidelberg, Germany, 1987; pp. 365–374.
16. Lan, T.; Pinnavaia, T.J. Clay-Reinforced Epoxy Nanocomposites. *Chem. Mater.* **1994**, *6*, 2216–2219. [[CrossRef](#)]
17. Tenório-Neto, E.T.; Lima, D.d.; Guilherme, M.R.; Lima-Tenório, M.K.; Scariot, D.B.; Nakamura, C.V.; Kunita, M.H.; Rubira, A.F. Synthesis and drug release profile of a dual-responsive poly (ethylene glycol) hydrogel nanocomposite. *RSC Adv.* **2017**, *7*, 27637–27644. [[CrossRef](#)]
18. Khan, M.S.J.; Khan, S.B.; Kamal, T.; Asiri, A.M. Agarose biopolymer coating on polyurethane sponge as host for catalytic silver metal nanoparticles. *Polym. Test.* **2019**, *78*, 105983. [[CrossRef](#)]
19. Kamal, T.; Ahmad, I.; Khan, S.B.; Asiri, A.M. Agar hydrogel supported metal nanoparticles catalyst for pollutants degradation in water, Desalin. *Water Treat.* **2018**, *136*, 290–298. [[CrossRef](#)]
20. Khan, M.S.J.; Kamal, T.; Ali, F.; Asiri, A.M.; Khan, S.B. Chitosan-coated polyurethane sponge supported metal nanoparticles for catalytic reduction of organic pollutants. *Int. J. Biol. Macromol.* **2019**, *132*, 772–783. [[CrossRef](#)]
21. Yadollahi, M.; Gholamali, I.; Namazi, H.; Aghazadeh, M. Synthesis and characterization of antibacterial carboxymethylcellulose/CuO bio-nanocomposite hydrogels. *Int. J. Biol. Macromol.* **2015**, *73*, 109–114. [[CrossRef](#)] [[PubMed](#)]
22. Hom, W.L.; Bhatia, S.R. Significant enhancement of elasticity in alginate-clay nanocomposite hydrogels with PEO-PPO-PEO copolymers. *Polymer* **2017**, *109*, 170–175. [[CrossRef](#)]
23. Rafieian, S.; Mirzadeh, H.; Mahdavi, H.; Masoumi, M.E. A review on nanocomposite hydrogels and their biomedical applications. *Sci. Eng. Compos. Mater.* **2019**, *26*, 154–174. [[CrossRef](#)]
24. Memic, A.; Alhadrami, H.A.; Hussain, M.A.; Aldhahri, M.; al Nowaiser, F.; Al-Hazmi, F.; Oklu, R.; Khademhosseini, A. Hydrogels 2.0: Improved properties with nanomaterial composites for biomedical applications. *Biomed. Mater.* **2015**, *11*, 014104. [[CrossRef](#)] [[PubMed](#)]
25. Phan, V.G.; Thambi, T.; Gil, M.S.; Lee, D.S. Temperature and pH-sensitive injectable hydrogels based on poly (sulfamethazine carbonate urethane) for sustained delivery of cationic proteins. *Polymer* **2017**, *109*, 38–48. [[CrossRef](#)]
26. Barkhordari, S.; Yadollahi, M.; Namazi, H. pH sensitive nanocomposite hydrogel beads based on carboxymethyl cellulose/layered double hydroxide as drug delivery systems. *J. Polym. Res.* **2014**, *21*, 454. [[CrossRef](#)]
27. Pagonis, K.; Bokias, G. Temperature- and solvent-sensitive hydrogels based on N-isopropylacrylamide and N,N-dimethylacrylamide. *Polym. Bull.* **2007**, *58*, 289–294. [[CrossRef](#)]
28. Haider, A.; Haider, S.; Kang, I.-K.; Kumar, A.; Kummara, M.R.; Kamal, T.; Han, S.S. A novel use of cellulose based filter paper containing silver nanoparticles for its potential application as wound dressing agent. *Int. J. Biol. Macromol.* **2018**, *108*, 455–461. [[CrossRef](#)] [[PubMed](#)]
29. Mahdavinia, G.R.; Mousavi, S.B.; Karimi, F.; Marandi, G.B.; Garabaghi, H.; Shahabvand, S. Synthesis of porous poly (acrylamide) hydrogels using calcium carbonate and its application for slow release of potassium nitrate. *Express Polym. Lett.* **2009**, *3*, 279–285. [[CrossRef](#)]

30. Kamal, T.; Anwar, Y.; Khan, S.B.; Chani, M.T.S.; Asiri, A.M. Dye adsorption and bactericidal properties of TiO<sub>2</sub>/chitosan coating layer. *Carbohydr. Polym.* **2016**, *148*, 153–160. [[CrossRef](#)]
31. Ahmad, I.; Khan, S.B.; Kamal, T.; Asiri, A.M. Visible light activated degradation of organic pollutants using zinc-iron selenide. *J. Mol. Liq.* **2017**, *229*, 429–435. [[CrossRef](#)]
32. Zhang, T.; Cheng, Q.; Ye, D.; Chang, C. Tunicate cellulose nanocrystals reinforced nanocomposite hydrogels comprised by hybrid cross-linked networks. *Carbohydr. Polym.* **2017**, *169*, 139–148. [[CrossRef](#)]
33. Zhang, T.; Zuo, T.; Hu, D.; Chang, C. Dual physically cross-linked nanocomposite hydrogels reinforced by tunicate cellulose nanocrystals with high toughness and good self-recoverability. *ACS Appl. Mater. Interfaces* **2017**, *9*, 24230–24237. [[CrossRef](#)] [[PubMed](#)]
34. Marandi, G.B.; Kermani, Z.P.; Kurdtabar, M. Fast and Efficient Removal of Cationic Dyes From Aqueous Solution by Collagen-Based Hydrogel Nanocomposites. *Polym. Plast. Technol. Eng.* **2013**, *52*, 310–318. [[CrossRef](#)]
35. Oryan, A.; Kamali, A.; Moshiri, A.; Baharvand, H.; Daemi, H. Chemical crosslinking of biopolymeric scaffolds: Current knowledge and future directions of crosslinked engineered bone scaffolds. *Int. J. Biol. Macromol.* **2018**, *107*, 678–688. [[CrossRef](#)] [[PubMed](#)]
36. Shankar, K.G.; Gostynska, N.; Montesi, M.; Panseri, S.; Sprio, S.; Kon, E.; Marcacci, M.; Tampieri, A.; Sandri, M. Investigation of different cross-linking approaches on 3D gelatin scaffolds for tissue engineering application: A comparative analysis. *Int. J. Biol. Macromol.* **2017**, *95*, 1199–1209. [[CrossRef](#)] [[PubMed](#)]
37. Bigi, A.; Cojazzi, G.; Panzavolta, S.; Rubini, K.; Roveri, N. Mechanical and thermal properties of gelatin films at different degrees of glutaraldehyde crosslinking. *Biomaterials* **2001**, *22*, 763–768. [[CrossRef](#)]
38. Gough, J.E.; Scotchford, C.A.; Downes, S. Cytotoxicity of glutaraldehyde crosslinked collagen/poly (vinyl alcohol) films is by the mechanism of apoptosis. *J. Biomed. Mater. Res. Off. J. Soc. Biomater. Jpn. Soc. Biomater. Aust. Soc. Biomater. Korean Soc. Biomater.* **2002**, *61*, 121–130. [[CrossRef](#)]
39. Bigi, A.; Cojazzi, G.; Panzavolta, S.; Roveri, N.; Rubini, K. Stabilization of gelatin films by crosslinking with genipin. *Biomaterials* **2002**, *23*, 4827–4832. [[CrossRef](#)]
40. Inoue, M.; Sasaki, M.; Nakasu, A.; Takayanagi, M.; Taguchi, T. An Antithrombogenic Citric Acid-Crosslinked Gelatin with Endothelialization Activity. *Adv. Healthc. Mater.* **2012**, *1*, 573–581. [[CrossRef](#)] [[PubMed](#)]
41. Kamal, T.; Khan, M.S.J.; Khan, S.B.; Asiri, A.M.; Chani, M.T.S.; Ullah, M.W. Silver Nanoparticles Embedded in Gelatin Biopolymer Hydrogel as Catalyst for Reductive Degradation of Pollutants. *J. Polym. Environ.* **2019**, *28*, 399–410. [[CrossRef](#)]
42. Luque, P.A.; Nava, O.; Soto-Robles, C.A.; Chinchillas-Chinchillas, M.J.; Garrafa-Garrafa, H.E.; Baez-Lopez, Y.A.; Valdez-Nunez, K.P.; Vilchis-Nestor, A.R.; Castro-Beltran, A. Improved photocatalytic efficiency of SnO<sub>2</sub> nanoparticles through green synthesis. *Optik* **2020**, *206*, 164299. [[CrossRef](#)]
43. Cheng, B.; Russell, J.M.; Shi, W.; Zhang, L.; Samulski, E.T. Large-scale, solution-phase growth of single-crystalline SnO<sub>2</sub> nanorods. *J. Am. Chem. Soc.* **2004**, *126*, 5972–5973. [[CrossRef](#)]
44. Zhang, J.; Ma, Z.; Jiang, W.; Zou, Y.; Wang, Y.; Lu, C. Sandwich-like CNTs@SnO<sub>2</sub> /SnO/Sn anodes on three-dimensional Ni foam substrate for lithium ion batteries. *J. Electroanal. Chem.* **2016**, *767*, 49–55. [[CrossRef](#)]
45. Ebrahimi, S.; Yunus, W.M.Z.W.; Kassim, A.; Zainal, Z. Synthesis of Nanocrystalline SnO<sub>x</sub> (x = 1–2) Thin Film Using a Chemical Bath Deposition Method with Improved Deposition Time, Temperature and pH. *Sensors* **2011**, *11*, 9207–9216. [[CrossRef](#)]
46. Hadia, N.M.A.; Ryabtsev, S.V.; Domashevskaya, E.P.; Seredin, P.V. Investigation of structural and optical properties of powder tin oxide (SnO<sub>x</sub>) annealed in air. *КОИДЕНСИРОВАНИЕ* **2009**, *7*, 10–15.
47. Santhi, K.; Rani, C.; Karuppuchamy, S. Synthesis and characterization of a novel SnO/SnO<sub>2</sub> hybrid photocatalyst. *J. Alloy. Compd.* **2016**, *662*, 102–107. [[CrossRef](#)]
48. Liang, H.; Raitano, J.M.; Zhang, L.; Chan, S.-W. Controlled synthesis of Co<sub>3</sub>O<sub>4</sub> nanopolyhedrons and nanosheets at low temperature. *Chem. Commun.* **2009**, *48*, 7569–7571. [[CrossRef](#)]
49. Sahoo, S.; Satpati, A.K. Electrochemical capacitance properties of cobalt oxide entangled over MWCNT and cobalt oxide AC composites. *J. Electroanal. Chem.* **2017**, *801*, 416–424. [[CrossRef](#)]
50. Ahmad, I.; Kamal, T.; Khan, S.B.; Asiri, A.M. An efficient and easily retrievable dip catalyst based on silver nanoparticles/chitosan-coated cellulose filter paper. *Cellulose* **2016**, *23*, 3577–3588. [[CrossRef](#)]
51. Ahmed, M.S.; Kamal, T.; Khan, S.A.; Anwar, Y.; Saeed, M.T.; Asiri, A.M.; Khan, S.B. Assessment of Anti-bacterial Ni-Al/chitosan Composite Spheres for Adsorption Assisted Photo-Degradation of Organic Pollutants. *Curr. Nanosci.* **2016**, *12*, 569–575. [[CrossRef](#)]
52. Ali, F.; Khan, S.B.; Kamal, T.; Anwar, Y.; Alamry, K.A.; Asiri, A.M. Bactericidal and catalytic performance of green nanocomposite based on chitosan/carbon black fiber supported monometallic and bimetallic nanoparticles. *Chemosphere* **2017**, *188*, 588–598. [[CrossRef](#)]
53. Ul-Islam, M.; Ullah, M.W.; Khan, S.; Kamal, T.; Ul-Islam, S.; Shah, N.; Park, J.K. Recent Advancement in Cellulose based Nanocomposite for Addressing Environmental Challenges. *Recent Pat. Nanotechn.* **2016**, *10*, 169–180. [[CrossRef](#)]
54. Khan, S.A.; Khan, S.B.; Kamal, T.; Asiri, A.M.; Akhtar, K. Recent Development of Chitosan Nanocomposites for Environmental Applications. *Recent Pat. Nanotechn.* **2016**, *10*, 181–188. [[CrossRef](#)]
55. Khan, S.A.; Khan, S.B.; Kamal, T.; Yasir, M.; Asiri, A.M. Antibacterial nanocomposites based on chitosan/Co-MCM as a selective and efficient adsorbent for organic dyes. *Int. J. Biol. Macromol.* **2016**, *91*, 744–751. [[CrossRef](#)]

56. Khan, S.B.; Khan, S.A.; Marwani, H.M.; Bakhsh, E.M.; Anwar, Y.; Kamal, T.; Asiri, A.M.; Akhtar, K. Anti-bacterial PES-cellulose composite spheres: Dual character toward extraction and catalytic reduction of nitrophenol. *RSC Adv.* **2016**, *6*, 110077–110090. [[CrossRef](#)]
57. Lee, H.-S.; Lin, Y.-W. Permeation of Hair Dye Ingredients, p-Phenylenediamine and Aminophenol Isomers, through Protective Gloves. *Ann. Occup. Hyg.* **2009**, *53*, 289–296. [[CrossRef](#)]
58. Swathi, T.; Buvanewari, G. Application of NiCo<sub>2</sub>O<sub>4</sub> as a catalyst in the conversion of p-nitrophenol to p-aminophenol. *Mater. Lett.* **2008**, *62*, 3900–3902. [[CrossRef](#)]
59. Lu, H.; Yin, H.; Liu, Y.; Jiang, T.; Yu, L. Influence of support on catalytic activity of Ni catalysts in p-nitrophenol hydrogenation to p-aminophenol. *Catal. Commun.* **2008**, *10*, 313–316. [[CrossRef](#)]
60. Contreras-Cáceres, R.; Sánchez-Iglesias, A.; Karg, M.; Pastoriza-Santos, I.; Pérez-Juste, J.; Pacifico, J.; Hellweg, T.; Fernández-Barbero, A.; Liz-Marzán, L.M. Encapsulation and Growth of Gold Nanoparticles in Thermoresponsive Microgels. *Adv. Mater.* **2008**, *20*, 1666–1670. [[CrossRef](#)]
61. Kamal, T.; Khan, S.B.; Asiri, A.M. Nickel nanoparticles-chitosan composite coated cellulose filter paper: An efficient and easily recoverable dip-catalyst for pollutants degradation. *Environ. Pollut.* **2016**, *218*, 625–633. [[CrossRef](#)]
62. Kamal, T.; Khan, S.B.; Haider, S.; Alghamdi, Y.G.; Asiri, A.M. Thin layer chitosan-coated cellulose filter paper as substrate for immobilization of catalytic cobalt nanoparticles. *Int. J. Biol. Macromol.* **2017**, *104*, 56–62. [[CrossRef](#)]
63. Kamal, T.; Ahmad, I.; Khan, S.B.; Asiri, A.M. Synthesis and catalytic properties of silver nanoparticles supported on porous cellulose acetate sheets and wet-spun fibers. *Carbohydr. Polym.* **2017**, *157*, 294–302. [[CrossRef](#)]
64. Khan, F.U.; Khan, S.B.; Kamal, T.; Asiri, A.M.; Khan, I.U.; Akhtar, K. Novel combination of zero-valent Cu and Ag nanoparticles @ cellulose acetate nanocomposite for the reduction of 4-nitro phenol. *Int. J. Biol. Macromol.* **2017**, *102*, 868–877. [[CrossRef](#)]
65. Kamal, T.; Khan, S.B.; Asiri, A.M. Synthesis of zero-valent Cu nanoparticles in the chitosan coating layer on cellulose microfibrils: Evaluation of azo dyes catalytic reduction. *Cellulose* **2016**, *23*, 1911–1923. [[CrossRef](#)]
66. Jana, S.; Ghosh, S.K.; Nath, S.; Pande, S.; Praharaj, S.; Panigrahi, S.; Basu, S.; Endo, T.; Pal, T. Synthesis of silver nanoshell-coated cationic polystyrene beads: A solid phase catalyst for the reduction of 4-nitrophenol. *Appl. Catal. A Gen.* **2006**, *313*, 41–48. [[CrossRef](#)]
67. Mallick, K.; Witcomb, M.; Scurrrell, M. Silver nanoparticle catalysed redox reaction: An electron relay effect. *Mater. Chem. Phys.* **2006**, *97*, 283–287. [[CrossRef](#)]